JOURNAL OF COLLOID AND INTERFACE SCIENCE **183,** 356–364 (1996)
ARTICLE NO. 0557

Molecular Controls on Kaolinite Surface Charge

PATRICK V. BRADY,[1] RANDALL T. CYGAN, AND KATHRYN L. NAGY

Geochemistry Department, Sandia National Laboratories, Albuquerque, New Mexico 87185–0750

Received December 11, 1995; accepted June 11, 1996

pH-dependent, multisite, surface charge on kaolinite can be explained by proton donor–acceptor reactions occurring simultaneously on Si and Al sites exposed on basal planes and edges. Si site Brønsted acidity at the kaolinite–solution interface differs minimally from that of pure SiO_2, whereas Al site acidity increases appreciably over that of pure Al_2O_3. Increasing temperature decreases the pK values of Al and Si proton-exchange sites. Calculated site densities indicate either an elevated participation of edges or substantial contribution from basal planes in the development of surface charge. Independent evidence from scanning force microscopy points to a higher percentage of edge surface area due to thicker particles and basal surface steps than previously assumed. Thus, no basal plane participation is required to explain the site densities determined from proton adsorption isotherms. Molecular modeling of the proton-relaxed kaolinite structure has been used to establish the elevated acidity of edge Al sites and to independently confirm the crystal-chemical controls on surface reactivity.

INTRODUCTION

A mechanistic understanding of mineral–solution interface reactions is needed to predict the extent and nature of a host of geochemical and biogeochemical processes. The origins of surface acidity are particularly important as surface charging plays a pivotal role in determining chemical transport in soils and groundwaters. By accepting or donating protons hydroxylated mineral surfaces acquire charge and the potential to control the attachment of cations or anions, bacteria, and high- and low-molecular-weight organic molecules. Surface charging reactions also modify the rates of dissolution and growth of mineral surfaces.

While the Earth's crust consists primarily of multioxide aluminosilicates, the vast majority of experimental and theoretical attention has focused on simple (hydr)oxides of Si, Ti, Fe, and Al. Only recently has multioxide surface chemistry of primary silicates and clays been addressed in detail (1–3). Many factors obscure the crystal-chemical controls on multioxide surface charge: (1) There is no universally accepted way to sum up, or predict, the acidities of the components of a multioxide silicate. (2) Preferential leaching of components is widely observed [e.g., (4–6)], generally pH-dependent (5, 7), and therefore difficult to model. (3) Active site densities for dissolution and proton exchange are certain to be crystallographically determined [e.g., (9)], hence difficult to unravel from bulk measurements done on powders. (4) Component acidities in the multioxide phase may differ greatly from their values in the single-oxide phase due to local crystal structure. Moreover, interface-controlled electron transfer reactions can greatly complicate the surface chemistry of Fe- and Mn-containing minerals.

Here we present measured kaolinite surface charge as a function of pH and temperature and advance a model for multisite acidity. Kaolinite is uniquely suited for examining multioxide surface chemistry because (1) it contains Al in octahedral coordination and Si in tetrahedral coordination with oxygen, two of the primary metal sites exposed at clay surfaces; (2) it has no interlayer cations that can be easily leached; (3) each (hydr)oxide component exists in two distinct structural environments at the surface (i.e., basal planes, edges); and (4) there is minimal substitution of variable-valence cations, hence, minor permanent structural charge. Effects of temperature were determined from 25 to 70°C because the geologic environments in which kaolinite surface interactions are important range from weathered outcrops and soils to subsurface sedimentary basins.

EXPERIMENTAL METHODS

pH and temperature-dependent surface charge were measured on a well-crystallized kaolinite (Clay Minerals Society source clay KGa1) from Washington County, Georgia, having a BET surface area of 10 to 11 $m^2\ g^{-1}$ (7, 10) in a background electrolyte of 0.1 *M* NaCl. No washing or aging of the kaolinite was carried out. This was done to avoid potentially complicating effects of aluminum and/or silica coatings observed to form in electrokinetic studies of clay minerals (11, 12). It is, however, recognized that the bulk chemical composition of KGa1 kaolinite is such that a few percent of impurities may be present (10). Pruett and Schroeder (13) showed that 0 to 0.5% Fe substitution for Al in octahedral sites may occur and 1 to 4% Al substitution

[1] To whom correspondence should be addressed.

0021-9797/96 $18.00

for Si in the ''soft'' Georgia kaolins, which include KGa1. The maximum values of these would indicate a maximum permanent charge of 35 mEq/100 g; however, the CEC for this kaolinite has been measured to be much less, 2 mEq/100 g (10) and 0.63 mEq/100 g (14), indicating minor substitution. Unpublished data of Robert Pruett (ECC, International) show that mineralogic impurities include 1.7% anatase, 0.02% Fe oxides, 0.1% micas, and trace quartz (15). The micas are predominantly muscovite about 10 to 100 μm in size. Even if we assume a maximum of 0.5% interstratified smectite based on chemistry alone and a CEC for this smectite of 100 mEq/100 g, we estimate only about 4 mEq/100 g total exchange capacity. This would correspond to a maximum CEC of 0.08 mEq/100 g. KGa1, unlike many other Georgia kaolins (16), is relatively pure and, as such, is considered of high quality for use in the paper industry.

The kaolinite was characterized using TEM and SFM. TEM images were obtained using a Phillips CM30 electron microscope operating at 300 kV. SFM images were obtained in air using a Park Scientific Instruments (PSI) Autoprobe LS in contact mode. A ''pinch'' of kaolinite was sonicated for 30 s in 3 ml of deionized water using an ultrasonicator at 50/60 Hz. We minimized the sonication time because excessive vibration has been shown to cleave kaolinite particles (17). A drop of the slurry was allowed to air-dry on a freshly cleaved muscovite mount. Images were obtained using PSI silicon Ultralevers, which have conical tips and high length-to-width aspect ratios. Ultralevers are sharper, although more delicate, than standard pyramidal Si_3N_4 tips and provide better resolution of step and edge features.

All solutions were made from doubly distilled water. The titrants for the adsorption measurements were 0.1 *M* NaOH and 0.1 *M* HCl (all solutions and standards were made from reagent-grade chemicals). pH electrodes (Mettler combination) were calibrated using NBS standards at the temperature of interest. Measurements were accurate to within 0.01 unit. Kaolinite (4.0 g) was titrated in 50 ml of electrolyte using a Mettler DL 12 titrator. Solutions were continuously stirred and N_2 was pumped directly into the solution for 15 min before and during each titration to purge the solution of CO_2. Temperature was held to ± 2°C by manually adjusting a hot plate and water jacket in which the reaction vessel was immersed. Generally 1 to 5 min elapsed between titrant additions (typically 0.01 ml), allowing pH readings to stabilize within a preselected tolerance. Adsorption equilibrium was presumed to exist when the pH changed by less than $\sim$0.01 unit per minute. After each titration the solutions were filtered and analyzed with a directly coupled plasma spectrometer for Al and Si. Dissolved levels of Al and Si were too small ($<$3 ppm, 1×10^{-4} mol liter^{-1}) to significantly impact the charge balance calculations below (this assumes that the observed Al and Si levels are not the result of rapid dissolution followed by sorption).

pH-dependent surface charge was calculated at each temperature by the relation

$$\sigma = (F/\mathrm{SA})([C_a - C_b] - [H^+] + [OH^-]), \quad [1]$$

where σ is the proton surface charge density (coulombs m^{-2}), F is Faraday's constant, SA is mineral surface area (m^2 liter^{-1}), and C_a and C_b are the amounts of acid and base titrant added (mol liter^{-1}), respectively. Note that [1] takes no account of any permanent charge arising from heterovalent substitution (see below).

KAOLINITE SURFACE CHEMISTRY

Surface charge on oxide minerals arises from the adsorption of water, hydroxyls, and protons to coordinatively unsaturated bonds. Measured kaolinite surface charge is heterogeneous in that it is the net of a number of reactions occurring on a variety of crystallographically distinct sites. The kaolinite unit cell is, simplistically, a gibbsite-like sheet of octahedrally coordinated Al bound to a sheet of silica tetrahedra through shared oxygens (18). Two of three octahedral sites are filled and the Al sheet is referred to as dioctahedral. Kaolinite layers, each comprising one octahedral and one tetrahedral sheet, are less tightly bound together in the *c* direction by hydrogen bonding between hydroxyl sites on the gibbsite basal plane and the highly electronegative oxygens of the silicon tetrahedral sheet (Fig. 1).

There is no universally accepted explanation for which group(s) controls pH-dependent adsorption and electrokinetic behavior in aqueous solutions. It may be the case that for different kaolinites, the predominant charged site or sites varies with bulk chemical composition or defect structure. Kaolinite surface charge has been ascribed to one, or a combination, of the following:

1. Si basal plane: Minor substitution of Al^{3+} or Fe^{3+} for Si^{4+} in the tetrahedral sheet would give rise to a small permanent (non-pH dependent) negative charge on the Si basal plane [e.g., (19–22)].

2. Edges: Exposed Al and Si centers at kaolinite edges are terminated by hydroxyls (19, 20), which, in the case of the aluminol, can accept or donate protons. Because alumina surfaces are generally positively charged at pH $<$ 8.7 [e.g., (23)], whereas silica mineral surfaces are anionic down to pH 2 to 3 [e.g., (24)], positive edge charge is attributed most reasonably to gibbsite-like edge sites (25). Negative surface charge is dominated at high pH (pH $>$ 9) by the contribution of silanol groups (25–27). Lewis acid sites also form due to the adsorption of water onto aluminol sites (28).

3. Basal plane hydroxyl groups: Hydroxyl groups on the octahedral plane are coordinated to two underlying aluminum atoms, and are thought to be appreciably less reactive

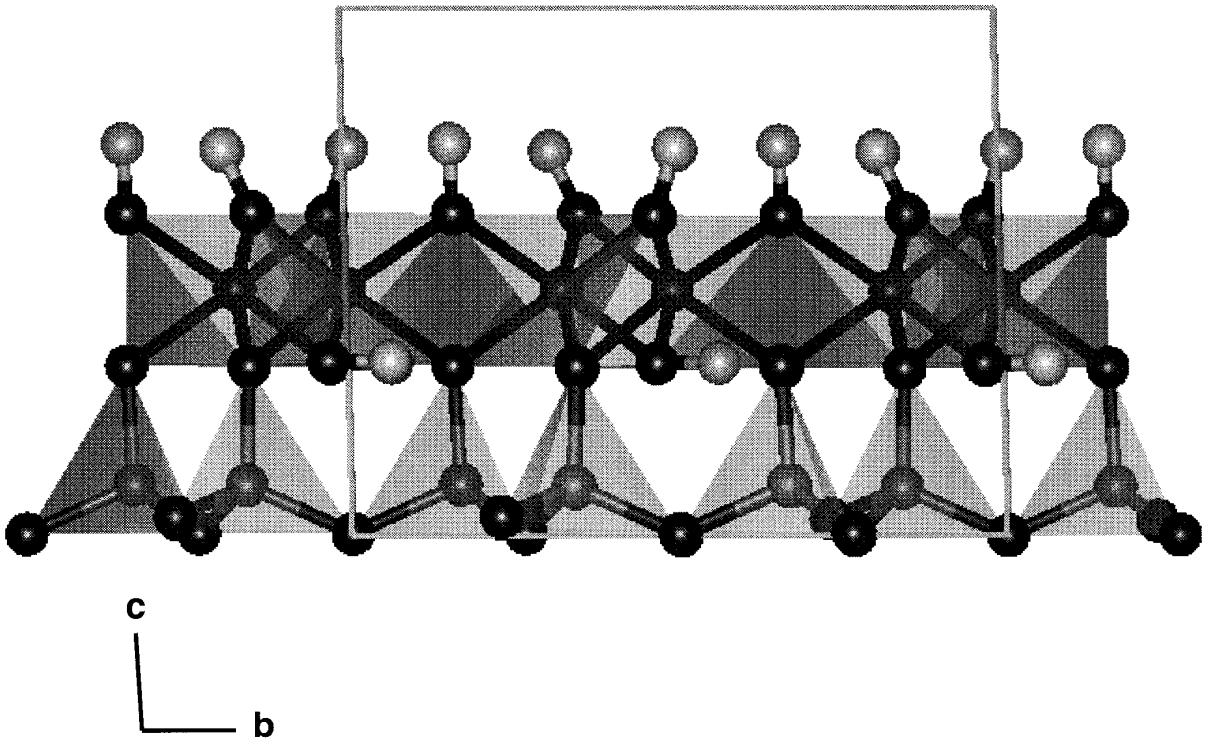

FIG. 1. Crystal structure of kaolinite based on the refinement of Bish (18). View is normal to the (100) face and the unit cell is denoted in gray. Silicon atoms are gray, aluminum atoms are dark gray, oxygen atoms are medium gray, and the hydrogen atoms are white.

than edge aluminols and silanols (28). Hydroxyl groups may exist locally on the silicon tetrahedral sheet as well [e.g., (1)]. Zhou and Gunter (29) have recently compared measured kaolinite surface charge with that of the constituent oxides SiO_2 and Al_2O_3 to argue for considerable ionization of basal planes.

4. Interlayer cations: Kaolinites often contain interstratified smectite layers that have interlayer cations (16, 30). These interlayer cations can easily be exchanged for protons in solution. The extent of smectite interstratification appears to be a function of the kaolinite's origin, although exact controls are unknown.

A variety of surface complexation models have been used to explain pH-dependent charge and the electrokinetic behavior of the kaolinite surface. Surface acidity and cation adsorption have been explained using the constant capacitance model (2, 31–33), the triple-layer model (26, 34), and semiempirical power-exchange functions (26).

MODELING APPROACH

Because the cation-exchange capacity of kaolinite is minimal at mildly acidic pH (26) we neglect any permanent, pH-independent, negative charge on the silicon tetrahedral face. This is consistent with the ion-exchange results of Ferris and Jepson (25). By neglecting permanent charge we are in effect examining kaolinite surface acidity solely by modeling the amphoteric properties of aluminol and silanol sites on the edges and basal planes.

The inclusion of basal planes in the model is required by the conclusion of Zhou and Gunter (29) that at best only a tenth of the pH-dependent surface charge can be fit onto kaolinite edges, assuming that edges contribute no more than 14% of the total kaolinite surface area. In other words, basal planes must possess pH-dependent negative surface charge as well. This points out the essence of the problem: if the acidity of the edges is appreciably different from that of basal planes, the areal distribution of the two must be known to accurately model total surface charge. Historically, the two types of acidity have been treated as one (26, 31, 32). Two exceptions are the studies by Zhou and Gunter (29) and Wieland and Stumm (2) in which the contributions of edges and basal planes were explicitly considered.

Our modeling strategy is three-pronged. We combined calculated charge distribution from potentiometric titration data, measured proportions of edge and basal surface area from SFM images, and modeled surface charge density using an atomistic approach to arrive at a consistent picture of the actual metal sites and locations that control surface charge development on kaolinite. The model is constrained by the conclusions we derived from the above studies, i.e., the permanent structural charge is small and charge on edges and basal surfaces is distinct.

The program FITEQL (35) was used to regress proton surface charge density measurements (calculated from Equation [1]) and provide best-fit values of surface site acidity constants as well as total site density, S_T. The latter was calculated using a relative error of 0.01 unit for pH (=0.02303 for $[H^+]$). FITEQL iteratively performs a nonlinear least-squares optimization calculation using an assumed chemical model of the solid solution interface. A constant capacitance model [e.g., (36, 37)] was used to link surface charge, σ, and surface potential, ψ. The capacitance was set to 4.0 F m^{-2}. This value was chosen to minimize the variance in the model fit to the data at 25°C.

Because the kaolinite surface is composed of Al and Si sites, a two-site model was used to fit the data. A four-site model ($Al_{edge} + Al_{basal} + Si_{edge} + Si_{basal}$) gave no discernible improvement in fit over the two-site model. In other words, the acidities of the edges and basal planes could not be differentiated on the basis of our experimental data. Therefore, as an initial hypothesis, we modeled surface charge development through reactions that were assumed to occur equivalently on edges and basal planes.

For aluminol groups,

$$\rangle Al—O—H_2^+ \leftrightarrow \rangle Al—O—H + H^+,$$

$$K_{Al,1} = [\rangle Al—O—H]\exp(F\psi/RT)\, a_{H^+}/[\rangle Al—O—H_2^+], \quad [2]$$

$$\rangle Al—O—H \leftrightarrow \rangle Al—O^- + H^+, \quad K_{Al,2} = [\rangle Al—O^-]\exp(-F\psi/RT)\, a_{H^+}/[\rangle Al—O—H]. \quad [3]$$

For silanol groups,

$$\rangle Si—O—H \leftrightarrow \rangle Si—O^- + H^+, \quad K_{Si,2} = [\rangle Si—O^-]\exp(-F\psi/RT)\, a_{H^+}/[\rangle Si—O—H]. \quad [4]$$

Bracketed terms are concentrations (mol m^{-2}). R and T are, respectively, the gas constant and temperature in Kelvin. We assumed that silanol groups do not protonate to become cationic at the pH values of the experiments. The very low pH_{zpc} of SiO_2 (pH 2–3) makes this a reasonable approach, and this has been assumed by previous workers (27).

pH-dependent kaolinite surface charge at 25, 50, and 70°C is shown in Fig. 2. The solid lines are best fits to the data from FITEQL. Regressed surface equilibrium constants (K, $pK = -\log K$) and site densities used to generate the solid lines are listed as a function of temperature in Table 1. Because there are few data points showing positive surface charge to attest to the presence of $\rangle Al—O—H_2^+$, $pK_{Al,1}$ can be expected to be somewhat linearly dependent on $pK_{Al,2}$ and $pK_{Si,2}$. The degree of this dependence is shown in Table 2, which gives the linear correlation coefficients between $pK_{Al,1}$ and the other variables that FITEQL adjusts. Best

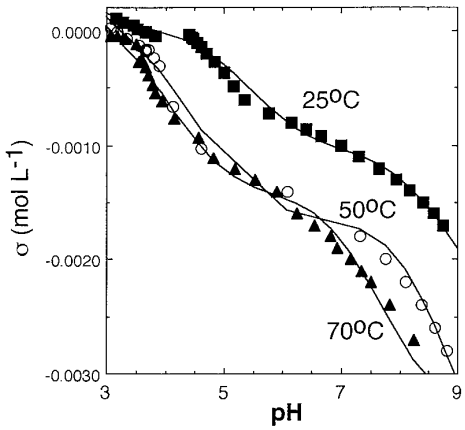

FIG. 2. Kaolinite surface charge at 25, 50, and 70°C in 0.1 *M* NaCl. Lines are best fits from FITEQL.

fits require at least 50% more Si sites than Al sites at all temperatures. There is no way to independently confirm this deviation from bulk stoichiometry because the actual ratio of the two types of sites exposed to solution will be a complex function of particle–particle interaction and any nonstoichiometric dissolution that occurred prior to the titrations. If we assume an initially stoichiometric exposed surface, the difference cannot be explained by nonstoichiometric leaching during the titrations because measured dissolved Al was too low (<3 ppm). Supporting evidence for this interpretation is provided by the study of Nagy *et al.* (38). They reported that XPS analyses of samples of a poorly crystalline kaolinite from Twiggs County, Georgia, that was untreated, dissolved and precipitated at pH 3 and 80°C, and submersed in 1 *N* HCl for 6 weeks at 25°C showed a surface Si/Al ratio of 0.96 ± 0.03, indicating minimal nonstoichiometric dissolution of kaolinite under a wide range of conditions.

There is a noticeable increase in calculated site densities with temperature, which may reflect production of edge surface with temperature [kaolinite dissolution rates increase with temperature; see Ref. (7)]. The shape of the 50°C titration curve differs somewhat from those of the 25 and 70°C curves, and there is a crossover with the latter at ~pH 6. This probably arises from the small number of data points (three) collected between pH 7 and 4 at 50°C.

Total site densities determined from the FITEQL analysis of 2.2 to 2.7 sites nm^{-2} (excluding the 50°C value of 7.8 μmol liter^{-1}) are so large as to point to participation of the basal planes in surface charging. With the exception of the 50°C, data uncertainties in fitted site densities are generally on the order of $2\sigma \sim 0.03$ site nm^{-2}. Edge site densities are estimated to be about 8 sites nm^{-2} if aluminol, silanol, and Lewis acid H_2O sites are counted (28). In addition, it is typically assumed that the proportion of a BET surface area attributable to edges is only about 0.08 to 0.2 (2, 28, 29). These estimates of percentage edge surface area are essentially based on geometric considerations, i.e., the particle

TABLE 1
Model Fit Parameters

T (°C)	$pK_{Al,1}$	$pK_{Al,2}$	$pK_{Si,2}$	$[\rangle Al—O—H]_T$[a]	$[\rangle Si—O—H]_T$[a]
25	2.33 (0.060)[b]	5.28 (0.014)	8.23 (0.064)	1.1 (0.02)	1.9 (0.01)
50	2.54 (0.056)	4.20 (0.028)	7.98 (0.152)	1.6 (0.04)	6.2 (1.75)
70	2.43 (0.076)	3.80 (0.030)	6.75 (0.050)	1.4 (0.03)	2.2 (0.09)

[a] mmol L^{-1}.
[b] In parentheses are calculated 2σ values.

thickness to diameter, or aspect, ratio. If only edges participate in proton adsorption, then at most 1.6 sites nm^{-2} are needed on the basal surfaces to account for all of the proton charge density measured (assuming that edges constitute 20% of the overall surface area). This presents somewhat of a dilemma, because it is generally considered that both the silicon tetrahedral and gibbsitic surfaces of kaolinite are relatively hydrophobic given that no bonds other than weak hydrogen bonds are broken when two kaolinite layers are separated. Therefore, we must find another way to account for the site densities observed from coulometric titration data. One reasonable explanation is that previous estimates of edge surface area are in error. For example, steps and ledges exposed on basal planes may provide additional edge sites that cannot be identified by geometric characterization of kaolinite particles from scanning or transmission electron photomicrographs.

To better quantify the amount of edge surface area, we determined geometric edge and basal surface areas of KGa1 particles from SFM images (Fig. 3). We found that the aspect ratio of this kaolinite ranges from 2:1 to 10:1. Interestingly, the particles tend to be thicker on average than previous estimates. In addition, the basal surfaces often contain steps that range from 1 to 30 unit cells high. For particularly rough particles (e.g., particle C in Fig. 3), the additional contribution from basal plane step edges approaches 5% of the particle's total geometric surface area. The percentage edge surface area ranges approximately from 10 to 50% of the total surface area. (In Fig. 3, we assumed that the underlying basal surfaces were perfectly flat; however, they too probably contain some basal step structure.) To explain the observed proton charge density of 2.2 to 2.7 sites nm^{-2} (again, excluding the 50°C value) we need from 27 to 34% edges, respectively, assuming that edge site density is 8 sites nm^{-2}, as determined by Sposito (28). Our SFM results show that KGa1 kaolinite easily contains this much edge surface area, based on examining only a few particles. The data also support site densities of up to ~3 sites nm^{-2} if we assume an average edge surface area of ~40%. Recently, Zhou and Maurice (39) reported on their SFM morphological characterization of KGa2 and KGa1-b kaolinites from Georgia. Their results support our data on KGa1 and suggest that, in general, edge surface areas assumed in previous studies (2, 29) have been somewhat underestimated. SFM analysis therefore indicates that basal surfaces need not be considered in modeling charge site densities on kaolinite, consistent with the concept of these surfaces behaving in a hydrophobic manner. Recent measurements of asphaltene adsorption onto kaolinite (40) point to 25 to 28% of the surface as being hydrophilic, supporting our hypothesis that edge sites make a larger contribution than most researchers have previously thought.

The results in Fig. 2 are consistent with previous measurements of kaolinite surface charge. Our measured 25°C zpc (pH 3.9–4.3) is slightly lower, yet similar to those measured by Riese (26) (pH 4.6) and Motta and Miranda (32) (pH 4.5). Also, fitting the 25°C data with the one-site model

TABLE 2
Correlation Coefficients for $pK_{Al,1}$ and Other Adjustable Parameters

T (°C)	$pK_{Al,1}$	$pK_{Al,2}$	$pK_{Si,2}$	$[\rangle Al—O—H]_T$	$[\rangle Si—O—H]_T$T
25	1.000	0.352	0.107	−0.209	−0.049
50	1.000	0.772	0.200	−0.379	−0.277
70	1.000	0.811	0.260	−0.465	−0.014

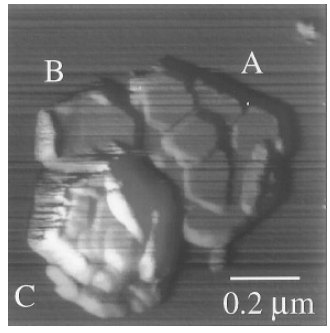

FIG. 3. Atomic force microscopy image of KGa-1 kaolinite particles. The gray flat background represents a height of 0 Å, and the brightest area in the NE quadrant of particle C is approximately 1200 Å high. Particle diameter ranges from 0.05 to 0.6 μm and particle thickness ranges from 100 to 1200 Å. *xyz* measurements of particle and major step dimensions were used to calculate total edge and basal surface areas for each kaolinite grain. The percentage edge surface area is (A) 13%, (B) 33%, and (C) 47%.

used by Motta and Miranda (32) gives values pK similar to those observed by the latter authors at 25°C.

Using a triple-layer model, but an otherwise identical approach to ours, Riese (26) argued for silanol group control over pH-dependent surface charge at acid to neutral pH and aluminol charge predominance at higher pH. Our model points in the opposite direction, namely, aluminol groups are proposed to control kaolinite surface charge at neutral and acidic pH values, with silanol groups contributing only under alkaline conditions. The potentiometric titration data allow either interpretation. Control over negative surface charge by Al sites at pH < 7 is hypothesized for a number of reasons. The value of $\Delta pK = pK_2 - pK_1$ for Al_2O_3 is relatively small [$\sim$4 (41)], whereas the ΔpK for SiO_2 is much larger [$>$7 (42)]. Assuming the same trend holds for the Al and Si sites on the kaolinite structure suggests that the lowest pK_2 belongs to the Al site (to give a ΔpK of $\sim$3) and that the Al site dominates overall deprotonation at pH < 7. The minimal temperature dependence observed for pK_1 is similar to that observed for Al oxide (43), pointing to Al control of positive surface charge. Schindler *et al.* (31) identified Al sites on kaolinite as the primary destination for sorbing Cu, Cd, and Pb from pH 4 to 7. At the same time XAS analysis of Co adsorption onto kaolinite (44) points to greater reactivity of Al sites (Al–O–H edge sites and bridging Al–O–Si sites) relative to Si–O–H sites. In general, surface charge becomes more negative with increasing temperature, and there is an increasing affinity of the kaolinite surface for cations.

Al sites at the kaolinite surface are appreciably more acidic than in pure alumina. The pH of zero charge for the Al sites on kaolinite is $\sim$3.8 at 25°C, compared with pH 8.55 for Al_2O_3 (42) and pH 8.9 for α-Al_2O_3 (45). Silanol sites, on the other hand, are only slightly less favored proton donors at the kaolinite surface relative to a pure silica phase, as p$K_{Si,2}$ is similar to the same quantity measured on pure SiO_2. The dependence of individual site acidity on the local crystal structure emphasizes the point that surface reactivity depends critically on interactions occurring at the molecular level.

To unravel the specific controls of site acidity at the kaolinite–water interface we used an atomistic approach based on the distribution of atomic charges and the observed crystallographic structure of kaolinite. A molecular representation of kaolinite including the basal and edge surfaces was constructed to perform these calculations. This form of molecular modeling relies on the net summation of charges at a given distance from a distribution of point charges to provide a molecular electrostatic potential (MEP) surface. The MEP calculation generates a solid surface about the kaolinite molecule using the van der Waals radii of the atoms. The surface is triangulated and the electrostatic potential V is evaluated at each vertex R of the polygonal surface:

$$V = \sum_{i=1}^{i=n} q(i)/|R - r(i)|, \qquad [5]$$

where n is the total number of atoms (ions), $q(i)$ is the charge of the ith atom, and $r(i)$ is the location of the ith atom relative to R. The MEP surface provides an indication of the electrostatic potential at the van der Waals surface as limited by the assumption of the point charge model. The point charge approximation may not be accurate if the electron density cannot be described as a spherical distribution about the atom; however, this is less a concern for silicate minerals with their predominantly ionic bonding component as compared with organic systems with significant covalent bonding. In essence, the MEP calculation provides the surface expression of the internal distribution of ionic charges associated with the molecule. The strength of the MEP surface calculation is in predicting the most favorable site on a molecular surface for a reaction that is initially driven by relatively long-range electrostatic forces, for example, sorption of solution ions and ionic complexes onto mineral surfaces.

The MEP calculation was performed on a UNIX workstation using the MEP surface algorithm provided through the Catalysis and Sorption Project software consortium and Molecular Simulations Inc. (San Diego, CA). The crystallographic refinement structure of Bish (18) was used to generate a kaolinite molecule composed of approximately 10 unit cells to represent a mineral two unit layers thick. The kaolinite molecule was generated to provide dangling oxygen atoms on the (100) and (010) surfaces that were subsequently protonated to satisfy silicon and aluminum valence requirements. This resulted in a molecule containing a total of 450 atoms. The (001) surfaces were terminated at the basal oxygens associated with the tetrahedral sheet and at the basal hydroxyls of the gibbsite-like octahedral surface. The singly protonated surfaces (one hydrogen per dangling oxygen) represent a kaolinite in equilibrium with a solution at approximately pH 4. Atomic charges were assigned using those obtained by the Mulliken analysis and periodic *ab initio* molecular orbital calculations of kaolinite by Hess and Saunders (46). Silicon has a charge of 2.5, aluminum 2.1, oxygen -1.2, and hydrogen 0.56. We assume that the atomic charge for edge protons is identical to that of the structural (inner and basal) hydrogens.

The positions of the hydrogens added to the cleaved (100) and (010) surfaces and the inner and basal hydrogens were energy optimized while constraining the other atomic positions to those determined by Bish (18). This was accomplished by evaluating the nonbonded interactions (coulombic and short-range Lennard-Jones energies) and oxygen–hydrogen bond forces using the Discover energy minimization code (Molecular Simulations Inc.). Force field parameters for the energy calculations were based on the consistent-valence force field (CVFF)

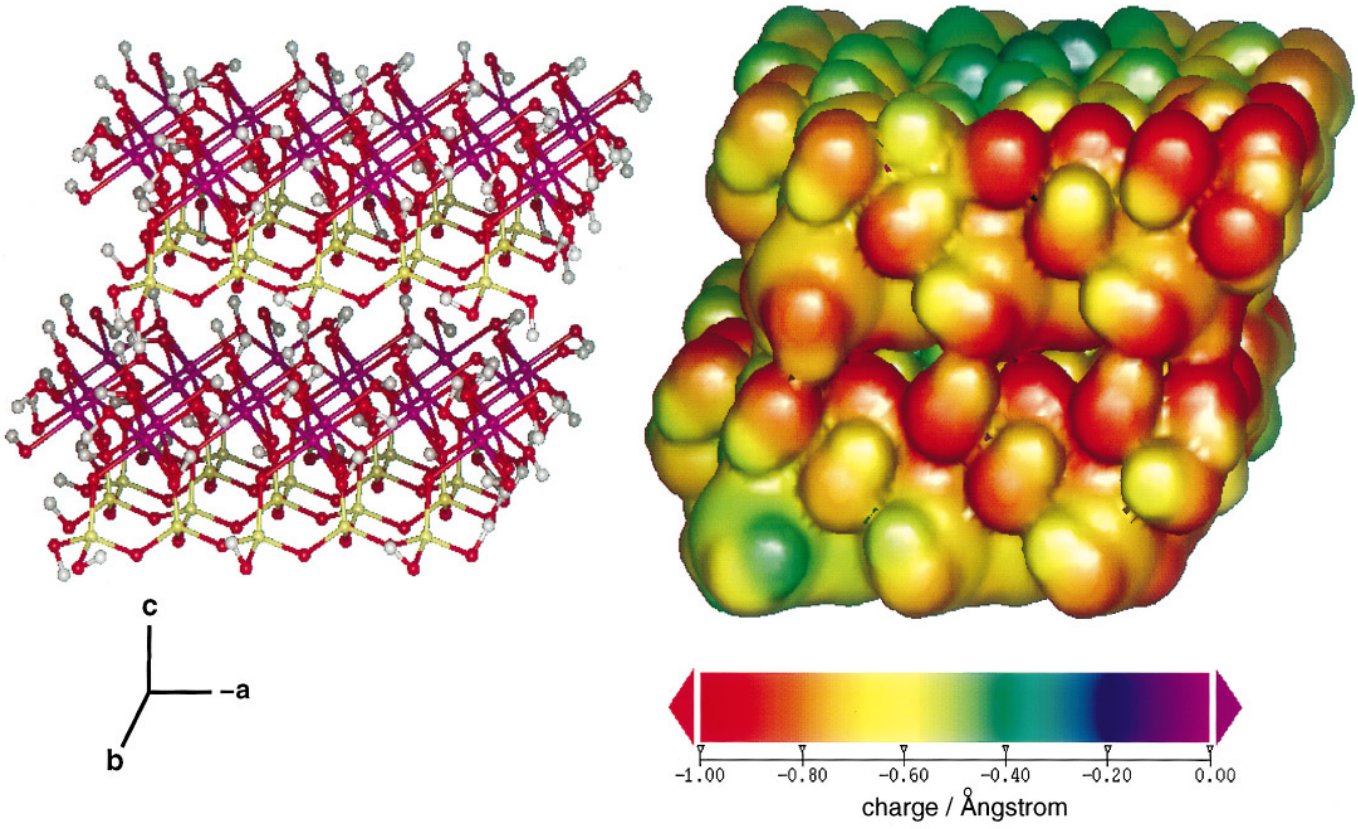

FIG. 4. Molecular electrostatic potential (MEP) surface (right) and corresponding structure (left) for a hydrated crystallite of kaolinite (silicon: yellow, aluminum: magenta, oxygen: red, hydrogen: white). Oblique view is approximately normal to the (010) surface of kaolinite; (001) basal surface is on top.

of Dauber-Osuthorpe *et al.* (47) that has been recently updated and parameterized by Molecular Simulations Inc. for crystalline silicate systems. Steepest descent and conjugate gradient numerical methods were used to evaluate potential energy trends and obtain the energy-optimized hydrogen positions for the kaolinite crystallite. The resulting molecular structure was then used for the MEP surface calculation.

The results of the MEP calculation indicate a significant difference between the edge and basal surfaces in their potential for surface reaction (Fig. 4). The (010) edge sites exhibit an extreme electrostatic potential that is approximately −0.9 charge/Å, whereas the (001) surface is characterized by an extreme value of −0.3 charge/Å. This sizable difference in electrostatic potential between the two kaolinite surfaces is related to the sheet structure of kaolinite and the net modification of the electrostatic potential by the spatial distribution of point charges. The MEP surface for the (010) surface of kaolinite exhibits the most negative potential at the aluminum octahedral layer between two of the upper protonated oxygens. This firmly suggests a stronger Lewis base behavior of these aluminum sites relative to the (001) basal aluminums and hydroxyl groups. The silicon tetrahedral layer exhibits a negative net MEP charge smaller in absolute value (−0.6 charge/Å) than that observed for the aluminum sites. The differences in potential exhibited in the MEP surface underscore the relative affinity of the different kaolinite surfaces and surface sites for subsequent reaction with an aqueous cation or positively charged complex. The spatial distribution of charge on the kaolinite surface will direct the initial approach of these species as influenced by long-range Coulombic forces.

Asymmetries in the MEP surface are related to crystallographic differences among the cleaved surfaces and to edge effects that result from limitations in the size of the kaolinite crystallite that is practical for the computational effort. Additionally, the surface hydrogen positions determined by the energy-minimization calculations are controlled by hydrogen bonding with oxygens between the aluminum and silicon layers and between kaolinite layers. The lack of long-range forces in these calculations emphasizes the influence of edge effects on these results.

DISCUSSION AND CONCLUSIONS

We had two primary conclusions:

1. Edge sites contribute more to kaolinite surface area

and charge development than has been assumed. One result of this is that basal plane ionization is not needed to account for measured proton adsorption.

2. Al sites at the kaolinite surface are significantly more acidic than are the same sites on the pure Al oxide, or Al hydroxide. Approaches that rely on simple addition of oxide components to understand multioxide surface charge (2, 7, 27, 33, 48, 49) are probably unrealistic at the molecular level, at least below pH 7. Nevertheless, the fact that Si site deprotonation is roughly the same for the kaolinite surface as the pure oxide suggests that at pH > 7, where Si surface charge is most important, the approximation may be more accurate.

Understanding proton adsorption is a necessary first step to unraveling the affinity of clay mineral surfaces for both inorganic and organic (biological and xenobiotic) species. The kaolinite results presented above suggest that the most important tools for understanding proton adsorption on clays are (1) analytical approaches for accurately quantifying the edge/basal plane ratio and (2) methods for quantifying the surface acidity shift of the non-Si oxides from the pure state to that in the clay lattice structure, as a function of mineral composition.

We have shown that scanning force microscopy is an effective solution for the first problem. Molecular modeling, as we have applied it to a fairly large molecular representation of a crystalline material, is uniquely suited for the second.

It is reasonable to apply the results obtained for the 1:1 layer phase kaolinite to examination of surface charge on the more complex 2:1 layer clays. In the latter, substitution of trivalent cations (primarily Fe and Al) into Si sites imparts a net negative charge to the basal plane which is satisfied by interlayer cations. The relative affinity of the basal plane for various cations reflects the interplay between electrostatic interaction and hydration effects (50). As a first approximation we would expect the same to hold true for cation interaction with heterovalently substituted sites at clay edges. Proton affinity for edge sites will ultimately depend on the radial distribution of charge among metal site, the adjacent basal planes, and the solution. A promising way to examine more complex clays, therefore, may be through the application of MEP calculations to establish charge distribution on these sites.

ACKNOWLEDGMENTS

We greatly appreciate the constructive comments of two anonymous reviewers and the support of the U. S. Nuclear Regulatory Commission and the U.S. Department of Energy Office of Basic Energy Sciences/Geoscience under Contract DE-AC04-94AL85000 to Sandia National Laboratories. P.V.B. thanks Dave Ward for back-seat driving on the surface complexation modeling. K.L.N. thanks Mike Dugger of Sandia National Laboratories for kind permission to use his AFM for the kaolinite morphology measurements. We also thank Robert Pruett, of ECC International, for permission to quote some of his analytical results on KGa-1.

REFERENCES

1. Stadler, M., and Schindler, P. W., *Clays Clay Minerals* **41,** 288 (1993).
2. Wieland, E., and Stumm, W., *Geochim. Cosmochim. Acta* **56,** 3339 (1992).
3. Kubicki, J. D., Blake, G. A., and Aplitz, S. E., *Am. Min.* **81,** 789 (1996).
4. Tamm, O., *Chem. Erde* **4,** 429 (1930).
5. Casey, W. H., Westrich, H. R., Arnold, G., and Banfield, J., *Geochim. Cosmochim. Acta* **53,** 821 (1989).
6. Hellmann, R., *Geochim. Cosmochim. Acta* **58,** 595 (1994).
7. Carroll-Webb, S. A., and Walther, J. V., *Geochim. Cosmochim. Acta* **52,** 2609 (1988).
8. Casey, W. H., and Bunker, B. *in* ''Mineral–Water Interface Geochemistry'' (M. F. Hochella and A. F. White, Eds.), Vol. **23,** p. 397. Mineralogical Society of America, 1990.
9. Lin, C. C., and Shen, P., *Geochim. Cosmochim. Acta* **57,** 27 (1993).
10. Van Olphen, H., and Fripiat, J. J. (1979) *in* ''Data Handbook for Clay Materials and other Non-metallic Minerals.'' Pergamon Press, New York.
11. Lyons, J. L., Furlong, D. N., and Healy, T. W., *Aust. J. Chem.* **34,** 1177 (1981).
12. Scales, P. J., Grieser, F., and Healy, T. W., *Langmuir* **6,** 582 (1990).
13. Pruett, R., and Schroeder, P. A. *Prog. Abs. of Clay Min. Soc. Mtg.* 103 (1995).
14. Schroth, B., and Sposito, G., *Clays Clay Minerals* in press (1996).
15. Pruett, R., personal communication (1995).
16. Lim, C. H., Jackson, M. L., Koons, R. D., and Helmke, P. A., *Clays Clay Minerals* **28,** 223 (1980).
17. Blum, A. E., *in* ''Scanning Probe Microscopy of Clay Minerals'' (K. L. Nagy and E. Blum, Eds.), Vol. 7, p. 172. Clay Minerals Society, 1994.
18. Bish, D. L., *Clays Clay Minerals* **41,** 738 (1993).
19. Schofield, R. K., and Samson, H. R., *Disc. Faraday Soc.* **18,** 138 (1954).
20. Cashen, G. H., *Trans. Faraday Soc.* **55,** 477 (1959).
21. Bolland, M. D. A., Posner, A. M., and Quirk, J. P., *Aust. J. Soil. Res.* **14,** 197 (1976).
22. Van Olphen, H., ''Clay Colloid Chemistry,'' 2nd ed. Wiley, New York, 1977.
23. Huang, C. P., and Stumm, W., *J. Colloid Interface Sci.* **43,** 409 (1973).
24. Parks, G. A., *in* ''Equilibrium Concepts in Natural Water Systems'' (W. Stumm, Ed.). Am. Chem. Soc., Washington, DC, 1967.
25. Ferris, A. P., and Jepson, W. B., *J. Colloid Interface Sci.* **51,** 245 (1975).
26. Riese, A. C., ''Adsorption of Radium and Thorium onto Quartz and Kaolinite: A Comparison of Solution/Surface Equilibria Models.'' Ph.D. thesis, Colorado School of Mines, Golden, CO, 1982.
27. Brady, P. V., and Walther, J. V., *Geochim. Cosmochim. Acta* **53,** 2823 (1989).
28. Sposito, G., ''The Surface Chemistry of Soils.'' Oxford Univ. Press, New York, 1984.
29. Zhou, Z., and Gunter, W. D., *Clays Clay Minerals* **40,** 365 (1992).
30. Kim, Y., Cygan, T. T., and Kirkpatrick, R. J., *Geochim. Cosmochim. Acta* **60,** 1041 (1996).
31. Schindler, P. W., Liechti, P., and Westall, J. C., *Neth. J. Agric. Sci.* **35,** 219 (1987).
32. Motta, M. M., and Miranda, C. F., *Soil Sci. Soc. Am.* **53,** 380 (1989).
33. Xie, Z., and Walther, J. V., *Geochim. Cosmochim. Acta* **56,** 3357 (1992).
34. Zachara, J. M., Cowan, C. E., Schmidt, R. L., and Ainsworth, C. C., *Clays Clay Minerals* **36,** 317 (1988).

35. Westall, J. C., ''FITEQL, A Computer Program for Determination of Chemical Equilibrium Constants from Experimental Data,'' Report 82-01. Chemistry Department, Oregon State Univ., Corvallis, 1982.
36. Schindler, P. W., and Gamsjäger, H., *Koll. Z. Ze. Polym.* **250,** 759 (1972).
37. Dzombak, D. A., and Morel, F. M. M. ''Surface Complexation Modeling: Hydrous Ferric Oxide.'' Wiley, New York, 1990.
38. Nagy, K. L., Blum, A. E., and Lasaga, A. C., *Am. J. Sci.* **291,** 649 (1991).
39. Zhou, Q., and Maurice, P. A., *in* ''V. M. Goldschmidt Conference Program and Abstracts,'' p. 102 (1995).
40. Saada, A., Siffert, B., and Papirer, E., *J. Colloid Interface Sci.* **174,** 185 (1995).
41. Katz, L. E., and Hayes, K. F., *J. Colloid Interface Sci.* **170,** 477 (1995).
42. Davis, J. A., and Leckie, J. O., *J. Colloid Interface Sci.* **63,** 480 (1978).
43. Brady, P. V., *Geochim. Cosmochim. Acta* **58,** 1213 (1993).
44. O'Day, P. A., Parks, G. A., and Brown, G. E., Jr., *Clays Clay Minerals* **42,** 337 (1994).
45. Hayes, K. F., Redden, G., Ela, W., and Leckie, J. O., *J. Colloid Interface Sci.* **142,** 448 (1991).
46. Hess, A. C., and Saunders, V. R., *J. Phys. Chem.* **96,** 4367 (1988).
47. Dauber-Osguthorpe, P., Roberts, V. A., Osguthorpe, D. J., Wolff, J., Genest, M., and Hagler, A. T., *Proteins Struct. Function Genet.* **4,** 31 (1988).
48. Guy, C., and Schott, J., *Chem. Geol.* **78,** 181 (1990).
49. Blum, A. E., and Lasaga, A. C., *Geochim. Cosmochim. Acta* **55,** 2193 (1991).
50. Eisenmann, G., *Biophys. J.* **2,** 259 (1962).